Numerical methods for radial solute transport to simulate uptake by plant roots

Abstract

The 1D radial solute transport model with non-linear inner boundary condition is widely used for simulating nutrient uptake by plant roots. When included into an architectural root model, this local model has to be solved for a high number of root segments, e. g. 10^5 – 10^6 segments for large root systems. Each root segment comes with its own local parameter set in heterogeneous root architectural models. Depending on the soil and solute, the effective diffusion coefficient spans over more than six orders (e. g. for N, K, and P). Thus a numerical implementation of this rhizosphere transport model is required to be fast, accurate and stable for a large parameter space.

We apply 13 methods to this rhizosphere model with root hairs and compare their accuracy, computational speed, and applicability. In particular, the Crank-Nicolson method is compared to higher-order explicit adaptive methods and some stiff solvers.

The Crank-Nicolson method sometimes oscillated and was up to a hundred times slower than an explicit adaptive scheme with similar accuracy. For a given spatial resolution, Crank-Nicolson had about one order lower accuracy as other tested methods. The maximum spatial time step can be estimated from root radius, solute diffusion, advection, and soil buffer power.

Although Crank-Nicolson is a viable method and often used as de-facto standard method for rhizosphere models, it was not the best performer in our comparison. While the best method remains problem specific, for general use in root architectural models we recommend adaptive Runge-Kutta with cubic or quadratic upwind for advection.

Keywords: Rhizosphere model, Barber-Cushman, Nye-Tinker, nutrient depletion, Runge-Kutta, Crank-Nicolson

1. Introduction

The radial rhizosphere model [1] has been widely used for simulating transport of various nutrients and their uptake by plant roots of many species. It was for example applied to phosphorus uptake by maize [2], zinc uptake by rice crop [3], magnesium, phosphorus, and potassium uptake by loblolly pine seedlings [4]

and N, P, K, Ca, Mg uptake by black cherry, northern red oak, and red maple [5]. Solving an individual instance of such a model typically takes a fraction of a second on modern CPUs. Advanced investigations in root biology require to take the soil heterogeneity, root system architecture and the variation in root parameters along that architecture into account. This can typically be done by replacing the simple root growth model with a 3D root architectural model, which discretizes the root system into millions of root segments, each with its own parameter set and instance of the radial rhizosphere model. This approach is for example implemented in Mai et al. [6] and in the functional structural plant model OpenSimRoot [7], which was used in several studies on the utility of root architectural and anatomical traits for uptake of phosphorus [8, 9, 10]. Thus, for simulations with 3D functional structural plant models such as OpenSimRoot, computational speed of the numerical implementation can become critical.

The rhizosphere model for a root segment consists of a 1D radial advection-diffusion equation with a Michaelis-Menten uptake kinetic at the inner boundary (rhizoplane) and zero flux outer boundary condition [1]. Itoh and Barber [11] added a reaction term describing uptake by root hairs. Though analytical solutions have been identified for various special cases of transport in the rhizosphere [12, 13, 14, 15, 16, 17, 18, 19], there is no analytical closed-form solution in the general case. Thus, in addition to computational speed, decisions on which method to use for an efficient numerical implementation should also be made on stability and accuracy. A certain minimum accuracy is desired over a range of model parameter values which typically is rather wide. For example, Bouldin [20] considered diffusion rates from 1×10^{-5} to $1 \times 10^{-9}\,\mathrm{cm^2\,s^{-1}}$ for phosphorus, however, without soil sorption, and root radii from 5×10^{-5} to $7.5 \times 10^{-4}\,\mathrm{cm}$ in a pure diffusion model without root competition. Relevant model parameters that determine nutrient depletion are soil parameters like solute diffusion, advection,

soil buffer power, along with root morphology, and uptake. Uptake by roots is governed by root radius, r_0, and Michaelis-Menten parameters describing the relation between concentration and nutrient uptake. Together, these parameters determine the concentration profiles and thus the suitability of specific numerical methods. How the parameter values relate to required minimum step sizes is hinted at by characteristic dimensionless numbers such as the Péclet number [e. g. 21], Courant number (CFL: Courant, Friedrichs, and Lewy [22]) and Fourier number [e. g. 23].

Plants not only absorb but also exude solutes. The model can be adapted for this by changing the inner boundary condition and introducing a reaction term to represent degradation rates of the (organic) exudates. Such adaptations benefit from flexibility in the implementation. Thus besides speed, accuracy, and stability, another requirement on the numerical implementation of the model is that it can be easily extended. Passioura and Frere [24], Nye and Marriott [25], Newman and Watson [26], Nye [27], Barber and Cushman [1], Itoh and Barber [11] used the (implicit) Crank-Nicolson method [28] to solve macroscopic rhizosphere nutrient transport and this method is still popular to solve such parabolic equations in rhizosphere models [e. g. 29]. Other commonly used methods are explicit forward simulations like a forward Euler method (FTCS: forward time central space) [e. g. 30, 31], which needs, in general, a much smaller time step size than the implicit Crank-Nicolson method (CN) to be stable and achieve comparable accuracy (for non-smooth solutions). Ou [19], Roose and Kirk [18] even used first-order (upwind) discretization for the first derivative in space and time, second-order only for the second derivative, and used the numerical results as a reference for the analytical approximations. Explicit methods might need smaller time steps but are straight forward to implement and easy to understand, which are helpful attributes when extending the model.

Numerical methods are a much overlooked topic in rhizosphere modeling in general. To our knowledge, so far no comprehensive testing of numerical methods for a classical rhizosphere model has been presented. Here, we investigated several explicit and implicit methods varying in their numerical order in space and time, applied to the classical rhizosphere model with root hairs by Itoh and Barber [11], concerning the mentioned criteria speed, accuracy, and applicability. We compared Crank-Nicolson to various explicit Runge-Kutta methods and implicit methods, BDF (Backward Differentiation Formulas) and IRK (implicit Runge-Kutta), with adaptive time steps. The aim was to identify methods that are most suitable for linking to a root architectural model, by fulfilling the criteria for a wide range of parameters, especially a high variation in the proportion of advection and effective diffusion. Numerical experiments with various parameters were performed to estimate the numerical error and computational time and thus to evaluate the different methods.

2. Methods

We describe the model by Itoh and Barber [11], different solution methods and their numerical discretizations. The various numerical methods compared in this study are listed in Table 1. This section also contains an explanation of the evaluation criteria used to compare the various methods.

2.1. Solute uptake model

Roots take up water and thereby create hydraulic gradients in the soil around them. The resulting flow of water transports solutes (nutrients) towards the roots. Unlike water, these solutes can not pass the cell membranes passively and apoplastic transport is blocked by the Casparian band. The solute concentration would simply increase at the root surface, however, plants have mechanisms to actively pump solutes into the root, typically at rates greater than the advective

Table 1: Discretization methods, abbreviations and their theoretical orders

Methods: Non-stiff solver		**Order** (total)	**Adv.**
Implicit (non-adaptive)			
Crank-Nicolson method	CN	$\mathcal{O}(\Delta r^2, \Delta t^2)$	$\mathcal{O}(\Delta r^2)$
Implicit Euler method, backward time central space	BTCS	$\mathcal{O}(\Delta r^2, \Delta t)$	$\mathcal{O}(\Delta r^2)$
Embedded explicit Runge-Kutta			
Cash-Karp, cubic upwind[c] adv., central diffusion	RKCK-CUI	$\mathcal{O}(\Delta r^2, \Delta t^5)$	$\mathcal{O}(\Delta r^3)$
Cash-Karp, central space	RKCK-CS	$\mathcal{O}(\Delta r^2, \Delta t^5)$	$\mathcal{O}(\Delta r^2)$
Cash-Karp, quadratic upwind[b] adv., central diffusion	RKCK-QUICK	$\mathcal{O}(\Delta r^2, \Delta t^5)$	$\mathcal{O}(\Delta r^2)$
Bogacki-Shampine, cubic upwind[c] adv., central diffusion	RK3(2)-CUI	$\mathcal{O}(\Delta r^2, \Delta t^3)$	$\mathcal{O}(\Delta r^3)$
Bogacki-Shampine, central space	RK3(2)-CS	$\mathcal{O}(\Delta r^2, \Delta t^3)$	$\mathcal{O}(\Delta r^2)$
Bogacki-Shampine, Koren flux limiter, 2^{nd}-order upwind[d] adv.	RK3(2)-koren	$\mathcal{O}(\Delta r^2, \Delta t^3)$	$\mathcal{O}(\Delta r^2)$
Methods: Stiff solver			
Embedded implicit Runge-Kutta			
Lobatto IIIA 2 (TR[a]), cubic upwind[c] adv., central diffusion	IRK2-CUI	$\mathcal{O}(\Delta r^2, \Delta t^2)$	$\mathcal{O}(\Delta r^3)$
Lobatto IIIA 2 (TR[a]), central space	IRK2-CS	$\mathcal{O}(\Delta r^2, \Delta t^2)$	$\mathcal{O}(\Delta r^2)$
Lobatto IIIC 4, central space	LobattoIIIC-CS	$\mathcal{O}(\Delta r^2, \Delta t^4)$	$\mathcal{O}(\Delta r^2)$
Implicit multi-step methods (adaptive)			
BDF 2-step, TR[a] start, cubic upwind[c] adv., central diffusion	BDF2-CUI	$\mathcal{O}(\Delta r^2, \Delta t^2)$	$\mathcal{O}(\Delta r^3)$
BDF 2-step, TR[a] start, central space	BDF2-CS	$\mathcal{O}(\Delta r^2, \Delta t^2)$	$\mathcal{O}(\Delta r^2)$

[a)]trapezoidal rule, [b)]QUICK ($\kappa = 1/2$), [c)]CUI ($\kappa = 1/3$), [d)]2^{nd}-order ($\kappa = -1$)

water flux. This effectively lowers the concentration at the root surface and causes diffusion of solutes towards the roots in addition to the advective flow. Thus, modeling nutrient uptake into a root system can be based on a partial differential equation (PDE) which includes advection (driven by water flux) and diffusion.

The transport model with root hairs [11] describes the change in solute concentration of the liquid phase, C [µmol cm^{-3}], in the rhizosphere around a segment of a root in radial coordinates:

$$\mathrm{b}\,\frac{\partial C}{\partial t} = \frac{1}{r}\frac{\partial}{\partial r}\left(rD\mathrm{b}\frac{\partial C}{\partial r} + r_0 v_0 C\right) - I_h. \tag{1}$$

Here, r_0 is the root radius and v_0 denotes the water flux at the root surface. Eq. (1) has to be solved between the root surface r_0 and an outer rhizosphere radius r_N, see the definition of boundary conditions below. Assuming radial symmetry around the root segment, solute concentration depends on one spatial coordinate r and time t, i.e. $C \coloneqq C(r,t)$. We will omit space and time dependence in some

notations for simplicity. The term $I_h \coloneqq I_h(r,t)$ [µmol cm^{-3} s^{-1}] accounts for root hair uptake by diffusion, modeled as instantaneous reaction for the root hairs at time t, see below. Note that Itoh and Barber [11] contains a typo causing the root hair term to be inside the differential operator. Soil buffer power, b, and effective diffusion coefficient, D [cm^2 s^{-1}], are adjusted to soil sorption by $D\mathrm{b} = D_\ell \theta \tau$, where D_ℓ is the diffusion rate in pure liquid, θ the volumetric water content and τ a tortuosity factor. These parameters are commonly assumed constant in rhizosphere modeling, at least locally. Spatial variations of b, D, and θ can be accounted for in root architectural models by assigning different values to different root segments. Temporal variations can be dealt with in a similar way, if the changes are slow compared to the time steps used for numerical integration. Here we stick to the common model assumption of locally constant D and b. In this case eq. (1) can be written as

$$\frac{\partial C}{\partial t} = a(r)\frac{\partial C}{\partial r} + D\frac{\partial^2 C}{\partial r^2} - \frac{I_h}{\mathrm{b}} \tag{2}$$

with a coefficient

$$a(r) \coloneqq \frac{1}{r}\left(D + \frac{v_0 r_0}{\mathrm{b}}\right). \tag{3}$$

Following Itoh and Barber [11], the solute uptake by root hairs is defined as

$$I_h(r,t) = \frac{I_{\max_h}(C_{rh}(r,t) - C_{\min})}{K_{\mathrm{m}_h} + C_{rh}(r,t) - C_{\min}} A_h(r), \tag{4}$$

with a maximum uptake flux for root hairs $I_{\max_h}$, a Michaelis-Menten constant for root hairs K_{m_h}, a lower limit for solute concentration $C_{\min}$, and the concentration at the root hair surface C_{rh}. The surface area of root hairs, A_h [cm^2 cm^{-3}], over

an interval δ along root hair length, per unit volume, is given by

$$A_h \coloneqq \begin{cases} \frac{2\pi r_h N_h \mathrm{L} \int_\delta dr}{2\pi \mathrm{L} \int_\delta r dr} = \frac{2 r_h N_h \delta}{(r+\delta)^2 - r^2} & \text{for } l_h + r_0 > r \\ 0 & \text{for } l_h + r_0 \leq r \end{cases} \tag{5}$$

The surface area per unit volume of root hairs used in eq. (4), $A_h(r)$, is obtained infinitesimally from eq. (5) by

$$A_h(r) \coloneqq \begin{cases} \lim_{\delta \to 0} \frac{2 r_h N_h \delta}{(r+\delta)^2 - r^2} = \frac{N_h r_h}{r} & \text{for } l_h + r_0 > r \\ 0 & \text{for } l_h + r_0 \leq r \end{cases} \tag{6}$$

Here, r_h and l_h [cm] are radius and length of the root hairs, respectively, and N_h [cm^{-1} root] denotes the number of root hairs in the calculation domain, i. e. on the root surface area over a unit root length L. The discrete formulations are described in section 2.3.3.

An approximation of the relation between the solute concentration at root hairs, $C_{rh}(r,t)$, and the average solute concentration in the rhizosphere, $C(r,t)$, was established by Baldwin et al. [32]:

$$C(r,t) \approx C_{rh}(r,t) \left(1 + \frac{\alpha_h r_h}{D\mathrm{b}} \ln\left(\frac{r_{h1}}{\exp(0.5) r_h}\right)\right), \tag{7}$$

where α_h is the root-hair absorbing power. This relation is valid if the root hair diameter is small compared to the mean distance between root hairs. The pairwise root hair half-distance is here calculated by $r_{h1} = \sqrt{r\pi \mathrm{L}/(2 N_h \mathrm{L})}$, assuming an equidistant root hair distribution. Substituting $\alpha_h C_{rh}$ by a Michaelis-Menten formula related to root-hairs [11], eq. (7) becomes

$$C(r,t) \approx C_{rh}(r,t) + \frac{I_{\max_h}(C_{rh}(r,t) - C_{\min})}{K_{\mathrm{m}_h} + C_{rh}(r,t) - C_{\min}} \frac{r_h}{D\mathrm{b}} \ln\left(\frac{r_{h1}}{\exp(0.5) r_h}\right). \tag{8}$$

Solving this equation for $C_{rh}(r,t)$ leads to an expression which can be inserted into eq. (4):

$$C_{rh}(r,t) \approx \mathrm{X} + \sqrt{\mathrm{X}^2 + C(r,t) \cdot (K_{\mathrm{m}_h} - C_{\min}) + \mathrm{Y} \cdot C_{\min}}\,, \tag{9}$$

using the abbreviations $\mathrm{Y} \coloneqq I_{\max_h}\left(\frac{r_h}{D\mathrm{b}} \ln\left(\frac{r_{h1}}{\exp(0.5) r_h}\right)\right)$ and $\mathrm{X} \coloneqq (C(r,t) - K_{\mathrm{m}_h} + C_{\min} - \mathrm{Y})/2$.

2.2. Boundary Conditions

Active uptake of solutes by the roots can be described by Michaelis-Menten kinetics in the boundary condition at the root surface r_0:

$$D\mathrm{b}\frac{\partial C(r_0,t)}{\partial r} + v_0 C(r_0,t) = \frac{I_{\max}(C(r_0,t) - C_{\min})}{K_{\mathrm{m}} + C(r_0,t) - C_{\min}}, \tag{10}$$

with a maximum uptake flux $I_{\max}$, the lower limit for solute concentration $C_{\min}$ already used in eq. (4), and a Michaelis-Menten constant K_{m}. This Robin boundary condition defines solute flow out of the domain at the r_0-boundary. The Michaelis-Menten kinetics introduces non-linearity into the otherwise linear PDE. Itoh and Barber [11] added a root hair term $I_h(r_0,t)$ to the right-hand-side of eq. (10) which we did not follow because it would give root hairs a too high weight on the total sink at r_0.

Roots compete with neighboring roots for nutrient resources. An average root competition over the whole root system can be taken into account by defining the outer boundary r_N as half of the averaged distance between roots and setting a zero-flux outer boundary condition. In this case, the length of r_N determines the amount of competition between roots. This zero-flux outer boundary condition reads

$$D\mathrm{b}\frac{\partial C(r_N,t)}{\partial r} + \frac{r_0 v_0}{r_N} C(r_N,t) = 0. \tag{11}$$

The initial condition at $t = 0$ was set to a start value $C(r, 0) = C_{\mathrm{init,r}}$ for all values of r.

2.3. Spatial Discretization

The spatial domain was discretized into N compartments, each with width Δr, such that $r_i = r_0 + i\,\Delta r$ for $i = 0, \ldots, N$. The diffusive term in eq. (2) was always discretized with a central finite difference, leading to second-order. For the inner spatial mesh points ($i = 1, \ldots, N-1$) this leads to

$$\frac{\partial C_i}{\partial t} = a(r)\frac{C^{(i)}_{\Delta r}}{\Delta r} + D\frac{C_{i-1} - 2C_i + C_{i+1}}{\Delta r^2} - \frac{I_{h,i}}{\mathrm{b}} + e \tag{12}$$

where $C_i \coloneqq C(r_i, t)$, $I_{h,i} \coloneqq I_h(r_i, t)$, and $C^{(i)}_{\Delta r}$ abbreviates a stencil of the first discrete derivative on the Δr-grid at node i, see below. The rest, e, contains errors of the assumptions of the analytical root hair solution and discretization in I_h and the truncation error, with the Landau-symbol $\mathcal{O}(\Delta r^2)$, from central differences.

For the boundaries at r_0 and r_N, special care has to be taken so that the accuracy is equal with the inner points. Otherwise, the global discretization order would be lower than stated in Table 1. Oosterlee et al. [33] pointed out that advection discretization should be $\mathcal{O}(\Delta r^2)$ accurate (at least for smooth parts) and monotone which can be realized by flux limiters. Next, we describe different methods used to discretize the first derivative in eq. (12).

2.3.1. Van Leer's scheme for the first spatial derivative

Van Leer's κ-scheme [34] for the first spatial derivative is [33]

$$C^{(i)}_{\Delta r} \coloneqq L^-_1 + L^-_\alpha + L^-_\beta + L^-_\gamma \tag{13}$$

with

$$L_1^- \coloneqq - C_i + C_{i+1}$$

$$L_\alpha^- \coloneqq - \frac{\kappa}{2}\left(-C_i + C_{i+1}\right)$$

$$L_\beta^- \coloneqq \frac{\kappa+1}{4}\left(-C_{i-1} + C_i\right)$$

$$L_\gamma^- \coloneqq \frac{\kappa-1}{4}\left(-C_{i+1} + C_{i+2}\right)$$

for $-a(r) < 0$, flow to the root ("downstream"), which is the usual case for rhizosphere models.

The order of above's scheme is at least $\mathcal{O}(\Delta r^2)$ for $-1 \leq \kappa \leq 1$ [35]. $\kappa = 1$ corresponds to central differences, $\kappa = 1/3$ is called CUI (cubic upwind interpolation), $\kappa = 1/2$ QUICK (quadratic upwind interpolation for advective kinematics), $\kappa = 0$ Fromm's scheme, and $\kappa = -1$ is the second-order upwind scheme [35]. We used mainly $\kappa = 1/3$, i. e.

$$C_{\Delta r}^{(i)} = -\frac{1}{3}C_{i-1} - \frac{1}{2}C_i + C_{i+1} - \frac{1}{6}C_{i+2},$$

for cases where we indicate the use of upwind discretization. And for the downstream discretization in RKCK-QUICK, the advection part is

$$C_{\Delta r}^{(i)} = -\frac{3}{8}C_{i-1} - \frac{3}{8}C_i + \frac{7}{8}C_{i+1} - \frac{1}{8}C_{i+2}.$$

2.3.2. Second-order upwind methods with flux limiter

We also implemented the "Koren" flux limiter method which is of order two and constructed to avoid oscillations at steep gradients [36]. A hybrid approach is considered by controlling an added artificial dissipation with a limiter ψ for

each time point. In this case, eq. (13) becomes [33]

$$C_{\Delta r}^{(i)} = L_1^- + \psi(R_i)\, L_\alpha^- + \psi(R_{i-1})\, L_\beta^- + \psi(R_{i+1})\, L_\gamma^-.$$

Smoothness is tested by

$$R_i = \frac{C_i - C_{i-1} + \epsilon}{C_{i+1} - C_i + \epsilon}.$$

with a constant ϵ to avoid division by zero, e. g., $\epsilon = 10^{-10}$ [36]. Koren [36] used a limiter $\psi(R_i) = \max\left(0, \min\left(2\, R_i, \left(1 + 2\, R_i\right)/3, 2\right)\right)$. We used this flux limiter together with the second-order upwind discretization, $\kappa = -1$, because of the smaller stencil and therefore ease of implementation at the boundary.

2.3.3. Discretization of uptake by root hairs

Uptake by root hairs, $I_{h,i}$, depends on $C(r_i, t)$ via the concentration at root hairs C_{rh} and on r_i via the surface area of root hairs per unit volume A_h given by eq. (6). Several possible ways to spatially discretize A_h can be developed. It can be either associated to the left neighboring node, to the right neighboring node or, as we did, mid-value:

$$A_{hi} = \frac{2N_h r_h \cdot \min(\Delta r, \max(0, l_h + r_0 - r_i + \frac{\Delta r}{2}))}{(r_i + \frac{\Delta r}{2})^2 - (r_i - \frac{\Delta r}{2})^2} \tag{14}$$

for $i = 1, \ldots, N-1$, and at the boundaries

$$A_{h0} = \frac{2N_h r_h \cdot \min(\frac{\Delta r}{2}, l_h)}{(r_0 + \frac{\Delta r}{2})^2 - r_0^2}, \tag{15}$$

$$A_{hN} = \frac{2N_h r_h \cdot \min(\frac{\Delta r}{2}, \max(0, l_h + r_0 - r_N + \frac{\Delta r}{2}))}{r_N^2 - (r_N - \frac{\Delta r}{2})^2}. \tag{16}$$

The three mentioned discretization variants are quite similar in total root uptake over time and depletion of concentration, for example, in the first compartment. However, the discretization associated to the right neighboring node will over-

estimate total cumulative uptake and thereby is least favorable. We chose the mid-value association because its $\mathcal{L}^1$-error of the root uptake is lowest and it needs lower spatial resolution (N) to converge to a total uptake value resulting from higher-resolution simulations.

The total uptake rate $\dot{U}(t)$ [µmol s^{-1}] over the discretized rhizosphere is the spatial sum of root hair uptake and root surface uptake,

$$\dot{U}(t) = \sum_{i=0}^{N} I_{hi}(t)\,\mathrm{V}_i + 2\pi r_0 \mathrm{L} \frac{I_{\max}(C_0(t) - C_{\min})}{K_\mathrm{m} + C_0(t) - C_{\min}}\,, \tag{17}$$

where V_i [cm^3] is the volume of the i-th compartment according to the discretization of eqs. (14)–(16), while I_h is a quantity per volume.

2.4. Time Discretization

Time was discretized into intervals Δt_j, such that $t_{j+1} = t_j + \Delta t_j$ for $j = 0, \dots N_t$, up to the simulation end time point t_end. For transient differential equations, e. g. Lecheler [37] recommends a higher-order (i. e. order ≥ 2) scheme.

2.4.1. Explicit and implicit Runge-Kutta

As explicit methods, embedded Runge-Kutta schemes were used for time discretization. The approach is a line-method where the differential equation is first discretized in one direction, giving a set of ordinary differential equations (ODEs) with initial value in time. The resulting autonomous ODE, $\partial C/\partial t = f(C)$, can be solved with a Runge-Kutta one-step solver. For eq. (12), the iterative formula of an s-stage Runge-Kutta method over time is:

$$C_{i,j+1} = C_{i,j} + \Delta t_j \sum_{m=1}^{s} b_m k_m \tag{18}$$

$$k_m = f(C_{i,j} + \Delta t_j \sum_{l=1}^{s} a_{ml}\, k_l) \tag{19}$$

where $C_{i,j} \coloneqq C(r_i, t_j)$, and a_{ml}, b_m are Runge-Kutta coefficients which can be found in Butcher-Tableaus. Here, a Runge-Kutta stage, k_m, is calculated over the spatial discretization and is not dependent on t explicitly.

Runge-Kutta methods can be made adaptive in a scheme with (embedded) evaluations of two successive orders [38]. The lower order solution is taken to approximate a local error for the step size control algorithm. We used third-order Bogacki-Shampine method, fifth-order Cash-Karp [39], and also two embedded implicit Runge-Kutta methods (IRK): Lobatto-IIIC of order 4 and Lobatto IIIA of order 2, the trapezoidal rule (IRK2). For the implicit Runge-Kutta methods we need to solve an $sN \times sN$-matrix system in each step which results from writing eq. (18) in implicit form: $\mathbf{F}(\mathbf{C_{j+1}}) = 0$. We solve this equation system for $C_{i,j+1}$ with Newton-Raphson iterations and for that allocate a Jacobian. For IRK2, the Jacobian has dimensions $N \times N$ and for Lobatto-IIIC ($s = 3$), $3N \times 3N$, which is a 3×3 block matrix of (sparse) banded $N \times N$ matrices. This block matrix $\mathbf{Q}$ has entries $q_{ml} = \mathbb{1}\delta_{ml} - \Delta t\, a_{ml} J_l$ where δ_{ml} is the Kronecker-Delta, $\mathbb{1}$ denotes the $N \times N$ identity matrix, and $J_l = [\partial f / \partial k_l]_{N \times N}$ are the derivatives. The resulting equation is $\mathbf{Q}_{j+1}^{k+1} \mathbf{d}_{j+1}^{k+1} = -\mathbf{F}_{j+1}^{k+1}$. We iteratively obtain solutions $\mathbf{d}_{j+1}^{k+1} = \mathbf{C}_{j+1}^{k+1} - \mathbf{C}_{j+1}^{k}$, where $\mathbf{C}_j = [C_{0,j}, \ldots, C_{n,j}]$, and k denotes a Newton iteration step. The stopping criterion $\|\mathbf{C}_{j+1}^{k+1} - \mathbf{C}_{j+1}^{k}\| < \textsc{aTol}$ is usually reached in a few iterations.

2.4.2. BDF

From the group of multi-step methods and as further stiff method alternative to IRK for the time stepping, we implemented the adaptive BDF-2 methods after [38, 40]. We did not use the time step algorithm used by Celaya et al. [40], but used the algorithm described in Appendix A for sake of comparability with the other adaptive methods. For the Jacobians of the implicit schemes, we used sparse matrices, implemented as three arrays containing the diagonal, upper-,

and lower-diagonal.

2.5. Crank-Nicolson and implicit Euler

The CN ($\Theta = 0.5$) and BTCS ($\Theta = 1$) methods are approaches of simultaneous discretization of time and space:

$$
\begin{aligned}
& C_{i,j+1} - \Theta\gamma_i \left(C_{i+1,j+1} - C_{i-1,j+1}\right) \\
& - \Theta\beta \left(C_{i-1,j+1} - 2C_{i,j+1} + C_{i+1,j+1}\right) - \Theta\frac{\Delta t}{\mathrm{b}} I_{h(i,j+1)} \\
& = C_{i,j} + (1-\Theta)\gamma_i \left(C_{i+1,j} - C_{i-1,j}\right) \\
& + (1-\Theta)\beta \left(C_{i-1,j} - 2C_{i,j} + C_{i+1,j}\right) + (1-\Theta)\frac{\Delta t}{\mathrm{b}} I_{h(i,j)}
\end{aligned} \tag{20}
$$

where $\beta \coloneqq D\Delta t/\Delta r^2$ and $\gamma_i \coloneqq a(r_i)\Delta t/(2\Delta r)$. The CN method is an implicit trapezoidal rule in time and a central finite difference scheme in space and hence can oscillate [41]. Both, CN and BTCS, are solved by Newton-Raphson scheme; the system matrix and Jacobian are described in Appendix B. CN is of order $\mathcal{O}(\Delta r^2) + \mathcal{O}(\Delta t^2)$, while BTCS is first-order in time.

2.6. Spatial and time step determination

The relation between advection and diffusion with respect to Δr is called (grid) Péclet number. For the i-th compartment it is $\mathrm{Pe}_i = a(r_i)\,\Delta r/D$. The grid Péclet number is relevant for the appropriate grid size (number of grid points) of a numerical method. Because of $r_0 < r_1 \cdots < r_N$, Pe_i has its maximum in the first compartment:

$$
\mathrm{Pe}_{\max} = \mathrm{Pe}_0 = \frac{\Delta r}{r_0}\left|1 + \frac{v_0 r_0}{D\mathrm{b}}\right| = \frac{\Delta r}{r_0}\left(1 + \mathrm{k}\right),
$$

for $v_0 > 0$, flow in root direction, and using a dimensionless ratio $\mathrm{k} \coloneqq r_0 v_0/(D\mathrm{b})$ of flux velocity, soil buffer power and effective diffusion. Thus, to maintain

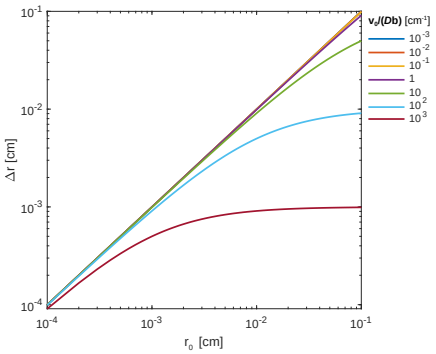

Figure 1: Maximal Δr to satisfy $\mathrm{Pe} \leq 1$, dependent on root radius r_0 for a range of orders of $\mathrm{k}/r_0 = v_0/(D\mathrm{b})$.

$\mathrm{Pe}_{\max} \leq \mathrm{c}$, the limit estimate of Δr is

$$\Delta r_{\max} = \frac{\mathrm{c} r_0}{1 + \mathrm{k}}, \tag{21}$$

which is a function of soil and root parameters. Thus, the root trait, r_0, sets a maximal limit to spatial grid resolution. Figure 1 shows how $\Delta r_{\max}$ depends on r_0 for different values of effective diffusion. Higher effective diffusion would accept coarser grids up to a limit, since $\Delta r_{\max} \to \mathrm{c}\, r_0$ for $\mathrm{k} \to 0$. For stability, it is often suggested that the grid Péclet number should be less than or equal 2, but for accuracy reasons, we took a limit of 1 instead of 2.

The CFL number, $|a(r)|\lambda$, is dependent on a mesh ratio, $\lambda := \Delta t/\Delta r$, and describes the relation of time step size of the advective transport part and spatial grid size. In explicit time-stepping this should be $\mathrm{CFL} \leq 1$ to prevent the physical solution to skip grid-cells in case of advective transport.

A solution propagation criterion for explicit methods with advection and dispersion is $\mathrm{CFL} + 2\,\mathrm{Fo}_m \leq 1$ [e. g. 42, p. 301], where Fo_m denotes the mass Fourier number. Together with the propagation by the inner boundary condition we used

$$\Delta t \leq \min\left(\frac{\Delta r \cdot \mathrm{b} \cdot K_{\mathrm{m}}}{I_{\max}}, \frac{\Delta r}{(1+\mathrm{k})D/r_0 + 2D/\Delta r}\right), \tag{22}$$

Table 2: Parameter set, modified from Barber [43].

		value	SI unit
Water flux	v_0	1×10^{-7}	$\mathrm{cm\,s^{-1}}$
Minimum solute concentration for uptake	$C_{\min}$	1×10^{-4}	$\mathrm{\mu mol\,cm^{-3}}$
Initial solute concentration in solution	$C_{\mathrm{init,r}}$	13.6×10^{-3}	$\mathrm{\mu mol\,cm^{-3}}$
Maximum uptake rate	$I_{\max}$	3.21×10^{-7}	$\mathrm{\mu mol\,cm^{-2}\,s^{-1}}$
Michaelis-Menten half-saturation constant	K_{m}	5.45×10^{-3}	$\mathrm{\mu mol\,cm^{-3}}$
Root radius	r_0	0.05	cm
Depletion zone boundary	r_N	1.05	cm
Simulated time period	t_{end}	10	d
Root hair radius	r_h	5×10^{-4}	cm
Number of root hairs on the surface of a unit segment	N_h	1000	$\mathrm{cm^{-1}}$
Average root hair length	l_h	0.2	cm
Soil buffer power	b	39	−
Unit length	L	1	cm

for all non-adaptive methods and as starting time step for adaptive methods. In the case of CN, the time step can, theoretically, be larger but oscillations occurred in some cases. The time step criterion in eq. (22) was used to ensure that CN was oscillation free. For all adaptive methods, we used the same step size control algorithm (Appendix A). This algorithm uses a relative error estimation in $\mathcal{L}^{\max}$-norm of the local truncation error. The tolerance limit of this step size error estimation was set to $\textsc{Tol} = 1 \times 10^{-4} = 0.01\,\%$. The absolute tolerance limit in $\mathcal{L}^2$-norm of a Newton-Raphson iteration step in implicit methods was set to $\textsc{aTol} = 1 \times 10^{-8}$. CPU-time was measured and related to a full (r, t) simulation run over an exemplary simulated time period of $t_{\mathrm{end}} = 10$ days (Table 2).

2.7. Error estimation

Each forward simulation was compared to its reference solution. The reference solutions were obtained with tolerances down to the relative machine accuracy and high spatial resolutions with negligible differences to even higher resolutions. To compare numerical results we used the relative $\mathcal{L}^1$ error norm (for non-

equidistant grids) as a measure, calculated as

$$\frac{\|\hat{u}-u\|}{\|u\|}=\frac{\sum_{j=0}^{N_t}\left(\left(|\hat{u}_j-u(t_j)|+|\hat{u}_{j+1}-u(t_{j+1})|\right)\frac{\Delta t_j}{2}\right)}{\sum_{j=0}^{N_t}\left(\left(|u(t_j)|+|u(t_{j+1})|\right)\frac{\Delta t_j}{2}\right)},$$

which is geometrically equivalent to a comparison of normalized numerical integrals of order one. Here, N_t is the number of time steps, $\hat{u}$ denotes the numerical solution at hand, and $u(t_j)$ evaluates the reference solution with spline-interpolation to compare the numerical solution with a pseudo exact solution. Note that, due to the setup of initial values, $\hat{u}_0 = u(t_0)$ for all methods. In the following, we used this relative $\mathcal{L}^1$ error norm for the total nutrient uptake rate by a root segment, $\dot{U}(t)$, which was calculated as uptake over root hair volume plus Michaelis-Menten uptake over the root surface, eq. 17. Total solute uptake rate, $\dot{U}(t)$, was taken for the comparison of numerical methods because it amplifies errors in the first compartment, $C(r_0, t)$, by about one order, leading to a higher sensitivity to numerical errors than concentration.

Mass conservation balances involve integration of mass over space and boundary fluxes over time, thus comparing two different numerical methods, each with their own numerical errors, and the balance calculation can be the least accurate one. For this reason we did not include a mass conservation balance into our comparison of methods.

2.8. Numerical experiments

Numerical experiments were performed over a range of depletion profiles (Figure 2). The different shapes resulted from varying the effective diffusion coefficient from $D = 1 \times 10^{-6}\,\mathrm{cm^2\,s^{-1}}$ to $D = 1 \times 10^{-11}\,\mathrm{cm^2\,s^{-1}}$. By varying the effective diffusion, a possible change in the soil buffer power was implied in

the diffusion coefficient. Barber [43] considered an effective diffusion coefficient of $D = 1 \times 10^{-12}\,\mathrm{cm^2\,s^{-1}}$ as minimum for bioavailability. Thus the variation in D covered an exemplary nutrient range of nitrogen, potassium, phosphorus to almost non-bioavailable solutes. The Michaelis-Menten parameters, $I_{\max}$ and K_m, for root and root hairs are set equal.

The root metabolic trait $I_{\max}$ (maximum uptake rate) influences the rhizosphere depletion profile similar to the effective diffusion D, see Figure 3, where $I_{\max}$ was varied between 1×10^{-5} and $1 \times 10^{-7}\,\mathrm{\mu mol\,cm^{-2}\,s^{-1}}$, in combination with two exemplary effective diffusion coefficients D. The range of the resulting shapes (Figure 3) is qualitatively similar (or in some cases even the same) to that obtained by varying the effective diffusion coefficient D in Figure 2, with low $I_{\max}$ corresponding to high D. Therefore we refrained from further investigating different values of $I_{\max}$ and focused on varying the effective diffusion coefficient D, with fixed b. This choice is also supported by the fact that the model is over-parameterized with respect to the solute concentration: if the soil buffer power, b_1, changes with a factor w such that $\mathrm{b}_2 = w\mathrm{b}_1$, we can have the same depletion profile of the solute concentration, with accordingly defined $I_{\max 2} = wI_{\max 1}$ and $v_{02} = wv_{01}$ (subscripts 1 and 2 denote unscaled and scaled parameters). Effective diffusion has to stay the same, $D_2 = D_1$, whereas the diffusion in liquid, D_ℓ, changes accordingly, $D_{\ell 2} = wD_{\ell 1}$. Contrary to the solute concentration profile, the uptake rate $\dot{U}(t)$ scales with factor w.

We include advection, $v_0 > 0$. However, this model, eq. (1), is suitable for relatively small advection by water flux in the range of 0 to $2 \times 10^{-6}\,\mathrm{cm\,s^{-1}}$ [25]. In this range the concentration profiles are not very sensitive to v_0 given the parameters of Table 2. The parameter v_0 mainly affects the concentration at the outer boundary of the simulated rhizosphere domain, modeled as zero flux of solution concentration, Figure 4. Since our evaluation criteria (error of nutrient

uptake rate and CPU-time) are not sensitive to those concentrations we did not vary v_0 in our sensitivity analysis.

This work considers standard spatial grids for comparison of the methods as described above. The grid could be made non-equidistant. However, presetting one non-equidistant spatial grid would be unsuitable, because the location of the steepest gradient depends on parameters and time as illustrated by Figures 2–4. Instead of presetting, a variable Δr could be calculated to fulfil certain tolerance criteria, see e. g. Eigenberger and Butt [44] for CN in Cartesian coordinates. This adds spatial grid optimization to the solution routine, which we do not study.

For certain parameter sets our differential equations are stiff after the definition of Lambert [45]. These stiff problems are faster solved with stiff solvers, as other solvers need small time steps despite the smooth solution. Hence we also compared representative stiff solvers.

3. Results

We performed simulations with the parameter set of Table 2 and three exemplary values of the effective diffusion coefficient, $D = 1 \times 10^{-6}$, 5×10^{-9}, and $1 \times 10^{-11}\,\mathrm{cm^2\,s^{-1}}$. For the highest value of effective diffusion considered, the solution is flat and smooth (Figure 2a). With diminishing D, the differential equation becomes advection dominated, and the gradients become steep near the root especially in the first compartments in time and space (t_0, r_0), see Figure 2b–f. The shape of the results is influenced by I_h, the root hair uptake: the concentration profile is more s-shaped than the concave profile in simulations without root hairs.

The system is stiff [45] if effective diffusion is high compared to the uptake rate ($D > I_{\max}$) and advection is relatively small, resulting in flat depletion profiles

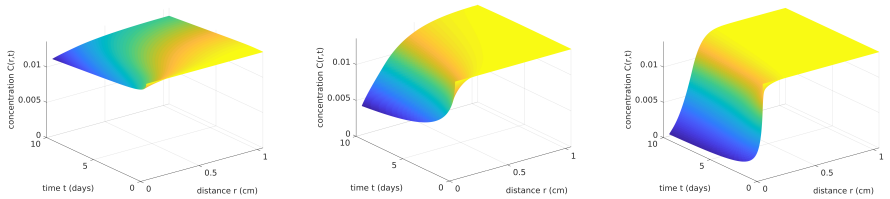

(a) $D = 1 \times 10^{-6}\,\mathrm{cm}^2\,\mathrm{s}^{-1}$ (b) $D = 1 \times 10^{-7}\,\mathrm{cm}^2\,\mathrm{s}^{-1}$ (c) $D = 1 \times 10^{-8}\,\mathrm{cm}^2\,\mathrm{s}^{-1}$

(d) $D = 1 \times 10^{-9}\,\mathrm{cm}^2\,\mathrm{s}^{-1}$ (e) $D = 1 \times 10^{-10}\,\mathrm{cm}^2\,\mathrm{s}^{-1}$ (f) $D = 1 \times 10^{-11}\,\mathrm{cm}^2\,\mathrm{s}^{-1}$

Figure 2: Three-dimensional mesh plots of solute concentrations in the rhizosphere over time and space for exemplary effective diffusion coefficients D varying over six orders. Other parameter values were taken as in Table 2. Plots may represent nitrate (a) potassium (b, c) phosphorus (d, e), and strongly bound phosphorus (f). The color varies by the quantity of the concentrations (z-axis). The curves start at the root surface $r = r_0$.

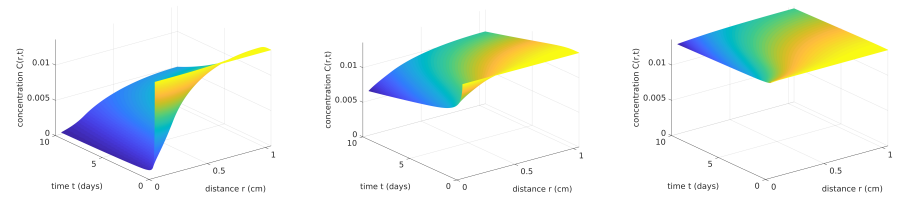

(a) $I_{\max} = 1 \times 10^{-5}$ mol cm^{-2} s^{-1}, $D = 1 \times 10^{-6}\,\mathrm{cm}^2\,\mathrm{s}^{-1}$ (b) $I_{\max} = 1 \times 10^{-6}$ mol cm^{-2} s^{-1}, $D = 1 \times 10^{-6}\,\mathrm{cm}^2\,\mathrm{s}^{-1}$ (c) $I_{\max} = 1 \times 10^{-7}$ mol cm^{-2} s^{-1}, $D = 1 \times 10^{-6}\,\mathrm{cm}^2\,\mathrm{s}^{-1}$

(d) $I_{\max} = 1 \times 10^{-5}$ mol cm^{-2} s^{-1}, $D = 1 \times 10^{-7}\,\mathrm{cm}^2\,\mathrm{s}^{-1}$ (e) $I_{\max} = 1 \times 10^{-6}$ mol cm^{-2} s^{-1}, $D = 1 \times 10^{-7}\,\mathrm{cm}^2\,\mathrm{s}^{-1}$ (f) $I_{\max} = 1 \times 10^{-7}$ mol cm^{-2} s^{-1}, $D = 1 \times 10^{-7}\,\mathrm{cm}^2\,\mathrm{s}^{-1}$

Figure 3: Three-dimensional mesh plots of solute concentrations in the rhizosphere over time and space for exemplary root uptake rates, represented by different values of $I_{\max}$, and example effective diffusion coefficients D. Other parameters were taken as in Table 2.

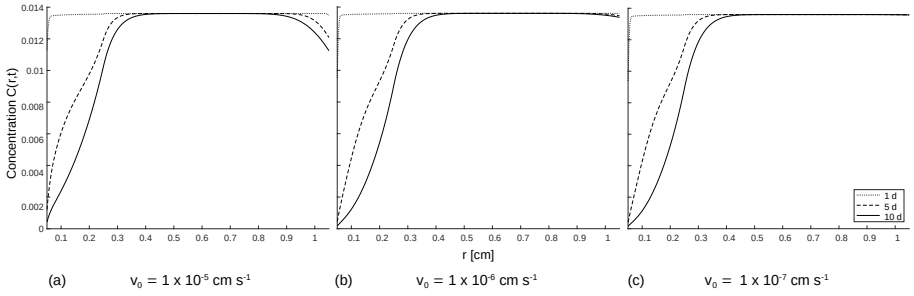

Figure 4: Solute concentrations in the rhizosphere over space at time points 1, 5, and 10 d for varying water flux v_0: (a) $1 \times 10^{-5}\,\mathrm{cm\,s^{-1}}$, (b) $1 \times 10^{-6}\,\mathrm{cm\,s^{-1}}$, (c) $1 \times 10^{-7}\,\mathrm{cm\,s^{-1}}$, for the example effective diffusion of $D = 5 \times 10^{-9}\,\mathrm{cm^2\,s^{-1}}$ and values of Table 2.

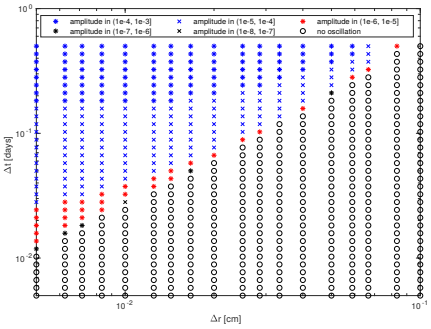

Figure 5: Oscillation amplitude ranges of CN for Δt-Δr-combinations for the example of $D = 1 \times 10^{-6}\,\mathrm{cm^2\,s^{-1}}$.

(Figures 2a, 3c and 3f). Also, stiffness of the system can lead to oscillations if the time step size is not changed appropriately with spatial resolution. Figure 5 shows the amplitude of such oscillations for CN in the case of high effective diffusion. Thus, the chosen parameter set influences not only the shape of the solution but also the stability of the method.

To compare the numerical methods of Table 1, the relative $\mathcal{L}^1$ error norm of total root uptake (Figure 6) and CPU-time (Figure 7) were monitored for the respective methods. Spatial resolution (given by N or Δr) and associated temporal resolution Δt were varied in a range appropriate to the respective scenario.

In Figure 6, the Péclet number is included, which sets a limit to the spatial resolution, see Figure 1. The low effective diffusion scenario (Figure 6c) with its steep depletion zone (Figure 2f) needed a finer grid than the high effective diffusion scenario (Figure 6a) to achieve similar accuracy.

There was no single method standing out from the others by high accuracy for all three scenarios (Table 3). There was a general tendency towards highest accuracy of explicit Runge-Kutta methods, yet IRK2-CUI showed best performance for the intermediate effective diffusion scenario ($D = 5 \times 10^{-9}\,\mathrm{cm^2\,s^{-1}}$) and fine spatial resolution (Figure 6b). In the low effective diffusion scenario (Figure 6c) the flux limiter method, RK3(2)-koren, gave more accurate results especially at coarser resolutions.

We desire methods that are both accurate and fast. For some methods improvements in accuracy come with relatively high increases in CPU-time, where others scale more favorably (Figure 7). The ranking of the methods according to CPU-time not only differed by accuracy but also by parameter space, here the effective diffusion coefficient. For the high effective diffusion scenario (Figure 7a), which could resemble nitrogen and is a stiff problem, the implicit adaptive

Table 3: Best performing methods by scenario and criteria.

Scenario	D $\mathrm{cm^2\,s^{-1}}$	**speed vs. accuracy**[a]	**accuracy vs. spatial resolution**[b]	nutrient example[c]
flat concentration profile	1×10^{-6}	IRK2-CUI, RKCK-CUI, RK3(2)-CUI	IRK2-koren, RKCK-CUI, RK3(2)-CUI	N
s-shaped concentration profile	5×10^{-9}	IRK2-CUI, RKCK-QUICK	IRK2-CUI, RKCK-QUICK	K
steep depletion zone	1×10^{-11}	RKCK-CUI	IRK2-koren, RKCK-CUI	P

a) Fig. 7, b) Fig. 6, c) soil sorption dependent. Abbreviations of methods according to Table 1.

trapezoidal integration (IRK2) and BDF were expected to be suitable, but the RK3(2)-CUI method showed a better performance. For the intermediate effective diffusion range (Figure 7b), which could resemble potassium, Runge-Kutta with upwind was in general fast while still accurate, having an error of under 0.1 % (third-order). Here, RKCK-QUICK was the fastest up to an accuracy where too many time steps were rejected. The non-linear CPU-time-increase of the explicit adaptive methods can be made linear by lowering the step size tolerance.

In Figure 7c, the low effective diffusion scenario, again explicit adaptive solvers worked best, whereas upwind methods were more accurate than the central difference schemes. RKCK-CUI and RKCK-QUICK performed comparably well in all three effective diffusion scenarios. BTCS and CN were slow in all scenarios for a given accuracy, suggesting that the 'default' choice for solving the 1D radial rhizosphere model might not be the most efficient one.

The error decreases with increasing grid size, therefore the similarity of Figures 7(d–f) to Figures 7(a–c). However, grid size can be important if memory consumption has to be optimized. Figures 7(d–f) show a steady pattern of the methods. The lines of the fixed-step methods, CN and BTCS, in Figures 7(d–f) did not change, because CPU to memory workload is the same for each scenario; the adaptive methods differ due to the number of time step rejections in a simulation.

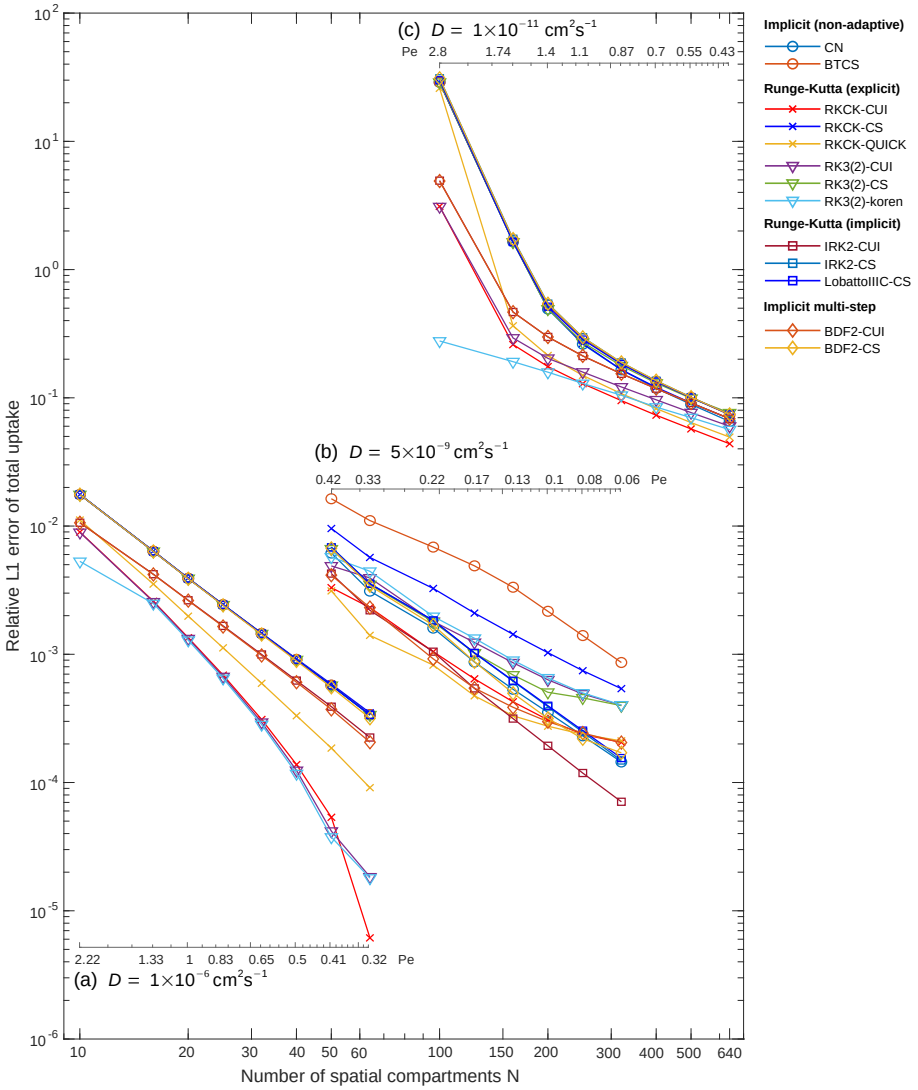

Figure 6: Minimal relative error of total root uptake for the 13 discretization methods of Table 1, related to spatial resolution and maximal grid Péclet number for three effective diffusion values (a) $D = 1 \times 10^{-6}$, (b) $D = 5 \times 10^{-9}$, (c) $D = 1 \times 10^{-11}\,\mathrm{cm}^2\,\mathrm{s}^{-1}$. All parameters except D were taken from Table 2. Abbreviations of methods according to Table 1.

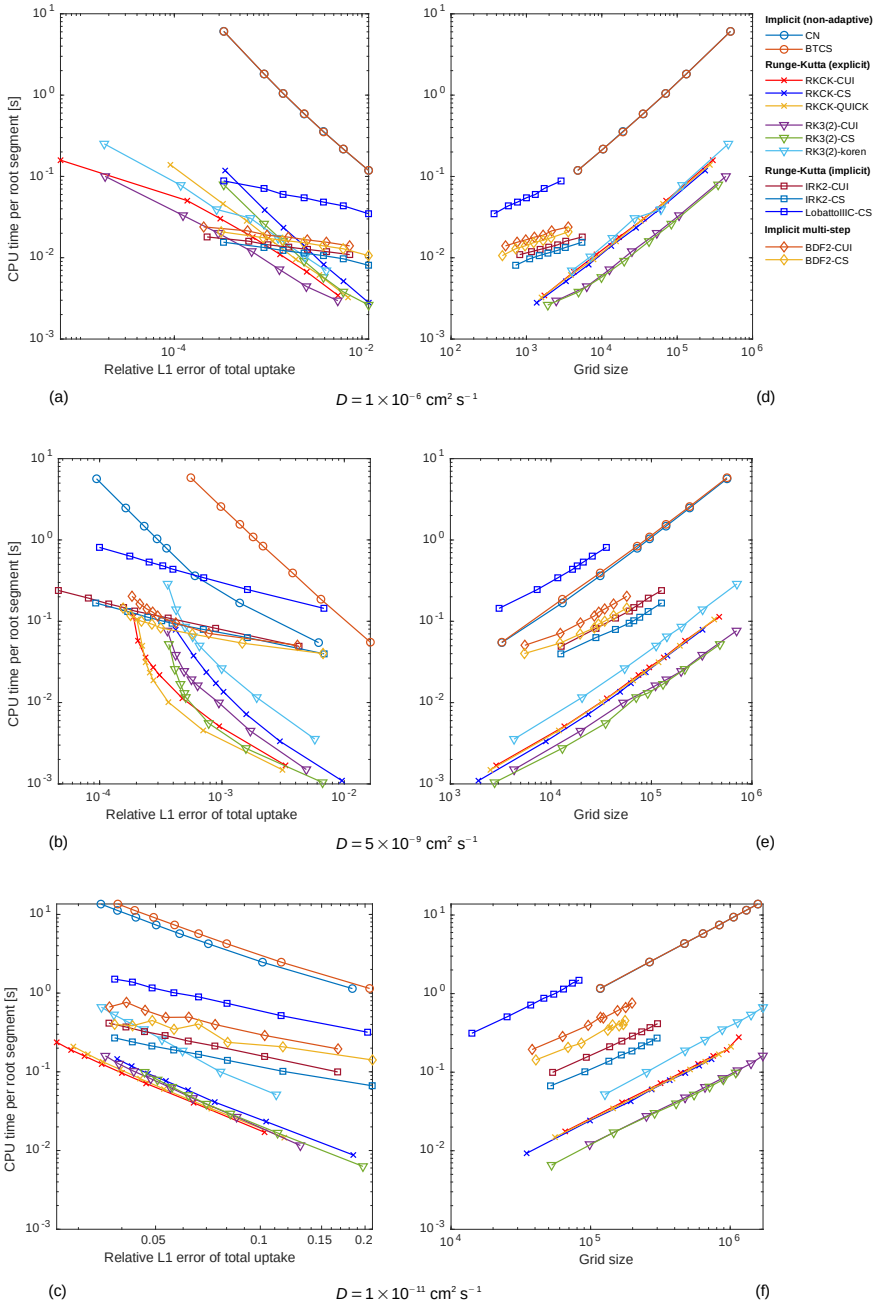

Figure 7: CPU-time compared to relative error and grid size (number of grid points) of different discretization methods. (a–c) Minimal relative error of total root uptake over time and runtime for spatial steps. (d–f) Spatial and temporal resolution compared to CPU-time. Grid size is defined by $N \times N_t$. All parameters except D were taken from Table 2. CN and BTCS are on top of each-other in (a), (d) and (f). A relative tolerance of 1×10^{-4} was used. Abbreviations of methods according to Table 1.

4. Discussion

We compared 13 numerical methods (Table 1) on the Itoh and Barber [11] model over a wide range of parameters. The methods cover a range of discretization types and orders, including explicit, implicit and stiff methods with and without upwind. The adaptive explicit methods included a flux limiter method and Runge-Kutta methods of different orders. We considered equidistant spatial discretization and higher-order κ-schemes, where steep gradients are still smoothed, but accuracy can be higher compared to first-order upwind.

In the simulations we considered flow into the root only. Upwind schemes have a direction in the discretization, so that water flux out of the root can be handled using a compact form which takes care of changing flow directions. This is of interest in a scenario where the sign of the v_0-term changes. In functional structural models, water uptake is no longer assumed to be constant and could change direction when, for example, hydraulic lift occurs at night.

Explicit methods are arguably easy to implement as they do not require to solve an equation system whose solving is the reason why the CN and BTCS method are slow. Thus explicit methods have the potential to be "fast", but will also use fine grids for sufficient accuracy. Consistent with Trottenberg et al. [35], the implicit central schemes are not as stable as the upwind schemes but can be faster in diffusion dominant cases. Upwind for advection is reasonable if the advection is dominant (Péclet number high) since discretization follows the flow direction. Central difference for diffusion leads to a conditionally stable scheme while for advection it is unconditionally unstable, hence we see in our simulations that added diffusion alleviates this effect. We used them for advection dominated scenarios (Table 1) for the sake of comparison. Adaptive methods can handle a large range of parameters and stabilize themselves in time by adapting the time step size. However, they are constrained by the local tolerance of the step

size control. CN, with its central differences, was implemented as in Barber and Cushman [1], Itoh and Barber [11]. It can be used on a wide range of parameters too, but needs in some limiting cases (very) fine resolution to reach similar accuracy as RK. Because of its implicit discretization, this adds to the computational time. CN can oscillate depending on the Fourier number [46]. Figure 5 illustrates the oscillations for CN and $D = 1 \times 10^{-6}\,\mathrm{cm^2\,s^{-1}}$. The Crank-Nicolson method has the advantage that it is unconditionally stable, but that holds theoretically only in the Euclidean norm and linear PDEs with homogeneous boundary conditions. In the maximum norm, it has a stability criterion [e. g. 47, 48]. The implicit Euler method (BTCS) is stable in both norms but has only first-order accuracy in time which is not sufficient in general. A first-order method (Euler method) is in general applicable for smooth solutions (here in time direction) and if step size restrictions are fulfilled. We do not consider it as universally applicable.

There is numerical diffusion in the upwind methods especially with first-order upwind, however, we used higher-order methods in space. For the rhizosphere transport problem considered here, a high soil buffer power (fast liquid-solid equilibration) helps stabilizing the numerical solution, hence there is no oscillation or significant smoothing for the upwind methods at steep solution fronts.

Providing a strategy to solve the 1D radial rhizosphere transport equation with root hairs in less computational time and for a wider range of parameters depends at least on the Péclet number and on the CFL condition, which control numerical dispersion. The CFL criterion was fulfilled in our simulations for the adaptive methods but in some grid-cells the Fourier number was larger than one.

We found that a finer grid is needed because of steep gradients in medium to low effective diffusion cases relative to advection (i. e. $v_0 r_0 > D\mathrm{b}$). Fine roots are computationally difficult as they need small Δr, similar to the low

effective diffusion examples. In advection dominant cases, the adaptive Runge-Kutta methods with second- or third-order upwind converge with reasonable computational effort whereas, in the case of low advection and high effective diffusion, the first derivative plays a minor role. If D is high relative to $I_{\max}$, the problem becomes stiff or moderately stiff and non-stiff methods need high time resolution because the adaptive step control algorithm rejects more time steps than supposed to be necessary for the smoothness of the solution. These high effective diffusion (and low uptake rate) scenarios greatly benefit from methods that are suitable for stiff differential equations such as BDF and implicit Runge-Kutta.

BDF is a multi-step method and we tested how the order of the starting step affects the error propagation since we simply did not want to start with a lower order. To our knowledge, an order one BDF as a starter, which is an implicit Euler, is often used for the starting step. We used the implicit trapezoidal rule here, while explicit RK starter and other methods are also possible. We found that accuracy is only slightly affected by a starter of order greater than two for BDF2.

An adaptive method can handle a wide parameter range and still maintains accuracy within its tolerance limits, but a small enough starting time step is needed, especially if the gradient at t_0 or the spatial resolution is high (hence the restrictions on the time step size). Such a high gradient is often present in rhizosphere models because a relatively high $I_{\max}$ can deplete the liquid phase quickly. The starting time step can be algorithmically estimated. However, this starting time step is not entitled to be optimal [38]. Therefore we used the starting time step similar to the fixed step, eq. (22).

A mathematically general statement about efficiency would need an $\mathcal{O}$-Notation analysis by counting $\mathcal{O}(1)$-operations. However, this is not practical for adaptive

methods. Therefore we used CPU-times as a measure of computational speed, being aware that absolute CPU-time measurements are hardware as well as software dependent. To ensure comparability of the CPU-times, we implemented function calls, such as Runge-Kutta steps, matrix constructions for the implicit schemes, and the step size control algorithm, in the same way for the numerical schemes. The computational time per time step in the explicit scheme is lower as the implicit scheme needs an equation system which is here solved by the Newton-Raphson method for each step, where the Jacobian of that equation system was built. However, for an implicit method, the time step can be larger. For solving the equation systems we used MATLAB's backslash operator, which was as efficient as our (tested) $\mathcal{O}(N)$ Thomas algorithm solver for tridiagonal systems. Memory-wise we stored the results for plotting and comparing. However, if only current time steps are needed, storage is simplified to vectors instead of matrices like in the architectural model OPENSIMROOT. This work led to a development of RKCK-CUI and RK3(2)-CUI in OPENSIMROOT which made the simulations more reliable for a wider range of scenarios and often faster.

5. Conclusion

We tested 13 different numerical methods to solve the 1D radial rhizosphere model for nutrient depletion and uptake. Our guiding question was how to solve the model most accurately and efficiently. We looked at the error of each method in the total root nutrient uptake rate over time, i. e. nutrient uptake by the root surface and root hairs, and compared the methods based on accuracy and CPU-time as a function of grid size. The effective diffusion coefficient was varied over a wide range in order to cover uptake of different nutrients such as nitrogen, potassium, phosphorus or even almost non-bioavailable solutes. The variation of effective diffusion led to different numerical challenges associated with the

different solute concentration profiles: from rather flat profiles but stiff problems for high effective diffusion to non-stiff problems with steep concentrations profiles at the root surface for low effective diffusion. Although CN became the standard in rhizosphere literature for solving a single component 1D rhizosphere model, it was slower by up to two orders and less accurate by up to one order compared to several other methods. We conclude that RKCK would be a better general-purpose method for simulating a wide range of parameters with high accuracy and low CPU-time.

Finding the best method is problem dependent, which means depending on mesh size, soil type, specific nutrient, and root radius. In a whole root simulation with changing conditions, a switch between schemes and mesh sizes based on the values of D, Péclet and CFL number is a possible strategy.

Appendix A. Step size control

A step size controlling algorithm for embedded Runge-Kutta methods [49, 38] is shown here, where p and q are the orders of the embedded Runge-Kutta methods, with $p > q$ and $error = \mathcal{O}(\Delta t^{(\min(p,q)+1)})$.

ALGORITHM: Step size control for embedded RK (pseudo code)

$facmin \leftarrow 0.5$ ▷ not more than two times reduction
$safety \leftarrow 0.9$ ▷ or other values
if $rejection \neq 1$ **then**
  $facmax \leftarrow 2$ ▷ usually between 1.5 and 5
else
  $facmax \leftarrow 1$ ▷ set $facmax = 1$ right after a step rejection
end if
if $error \leq$ TOL **then** ▷ continue with larger step
  $dt(j+1) \leftarrow \min(safety \cdot dt(j) \cdot (\frac{\text{TOL}}{error})^{\frac{1}{p}}, facmax \cdot dt(j))$
  if $dt(j+1) > h_{\max}$ **then**
    $dt(j+1) \leftarrow h_{\max}$
  end if
  $t \leftarrow t + dt(j)$
  if $t + dt(j+1) > T$ **then** ▷ T is simulation time interval, e. g. days
    $dt(j+1) \leftarrow T - t$
  end if

$j \leftarrow j + 1$
$rejection \leftarrow 0$
else ▷ repeat with smaller step
$dt(j) \leftarrow \max(safety \cdot dt(j) \cdot (\frac{\text{Tol}}{error})^{\frac{1}{q}}, facmin \cdot dt(j))$
if $dt(j) < h_{\min}$ **then**
$dt(j) \leftarrow h_{\min}$
end if
$rejection \leftarrow 1$
end if

Appendix B. Jacobian for CN and BTCS

CN ($\Theta = 0.5$) was implemented according to Itoh and Barber [11], Barber and Cushman [1] with added Θ to enable BTCS ($\Theta = 1$). Here we repeat the details of this implementation to include a comprehensive description of the derivatives of the root hair term. Eq. (20) can be rewritten as

$$\begin{aligned} &-S1_i\ C_{i-1,j+1} + D1\ C_{i,j+1} - S2_i\ C_{i+1,j+1} + Q1\ I_{h(i,j+1)} \\ &\qquad = P1_i\ C_{i-1,j} + D2\ C_{i,j} + P2_i\ C_{i+1,j} - Q2\ I_{h(i,j)}, \qquad i = 1, \ldots, n-1, \end{aligned}$$

with the abbreviations

$$\begin{aligned} S &:= (\Delta r/2) \cdot (1 + v_0 r_0/(D_e \mathrm{b})), \\ S1_i &:= \Theta(1 - S/r_i), & D1 &:= \Delta r^2/(D_e \Delta t) + 2\Theta, \\ S2_i &:= \Theta(1 + S/r_i), & D2 &:= \Delta r^2/(D_e \Delta t) - 2 \cdot (1 - \Theta), \\ P1_i &:= (1 - \Theta)(1 - S/r_i), & Q1 &:= \Theta \cdot \Delta r^2/(D_e \mathrm{b}), \\ P2_i &:= (1 - \Theta)(1 + S/r_i), & Q2 &:= (1 - \Theta) \cdot \Delta r^2/(D_e \mathrm{b}). \end{aligned}$$

Here $D1$ and $D2$ are similar to Itoh and Barber [11] but typo corrected, i. e. division instead of multiplication by Δt. For the inner ($i = 0$) and outer ($i = n$) boundaries eqs. (10) and (11), respectively, the ghost points $C_{-1,\cdot}$ and $C_{n+1,\cdot}$ outside of the computation domain are defined by

$$\begin{aligned} C_{-1,j} &= C_{1,j} - S3 \left(\frac{I_{\max}(C_{0,j} - C_{\min})}{K_{\mathrm{m}} + C_{0,j} - C_{\min}} - v_0 C_{0,j} \right), \\ C_{n+1,j} &= C_{n-1,j} - A1\ C_{n,j}, \end{aligned}$$

with $S3 := 2\Delta r/(D_e \mathrm{b})$ and $A1 := S3\ v_0 r_0/r_n$.

The discretized equation system $\mathbf{F} = 0$ is then given by

$$
\begin{aligned}
f_0 &= -2\Theta\ C_{1,j+1} + S1_0\ S3\left(\frac{I_{\max}(C_{0,j+1} - C_{\min})}{K_{\mathrm{m}} + C_{0,j+1} - C_{\min}} - v_0 C_{0,j+1}\right) \\
&\quad + D1\ C_{0,j+1} + Q1\ I_{h\,(0,j+1)} - P1_0\ C_{-1,j} - D2\ C_{0,j} - P2_0\ C_{1,j} + Q2\ I_{h\,(i,j)}, \\
f_{i\in[1,\ldots,n-1]} &= -S1_i\ C_{i-1,j+1} + D1\ C_{i,j+1} - S2_i\ C_{i+1,j+1} + Q1\ I_{h\,(i,j+1)} \\
&\quad - P1_i\ C_{i-1,j} - D2\ C_{i,j} - P2_i\ C_{i+1,j} + Q2\ I_{h\,(i,j)}, \\
f_n &= -2\Theta\ C_{n-1,j+1} + (D1 + S2_n\ A1)\ C_{n,j+1} + Q1\ I_{h\,(n,j+1)} \\
&\quad - P1_n\ C_{n-1,j} - D2\ C_{n,j} - P2_n\ C_{n+1,j} + Q2\ I_{h\,(n,j)}.
\end{aligned}
$$

The Jacobian $J(\mathbf{C}_{j+1})$ is tridiagonal of dimension $(n+1 \times n+1)$ with entries $[J_{i,k}] = \frac{\partial f_i(\mathbf{C})}{\partial C_{k,j+1}}$:

$$
\begin{aligned}
&[J_{0,0}] = f_0{}', && [J_{0,1}] = -2\Theta, \\
&[J_{n,n}] = D1 + S2_n\ A1 + Q1\ I'_{h\,(n,j+1)}, && [J_{n,n-1}] = -2\Theta, \\
&[J_{i,i}] = D1 + Q1\ I'_{h\,(i,j+1)}, && [J_{i,i-1}] = -S1_i, \qquad [J_{i,i+1}] = -S2_i,
\end{aligned}
$$

for $(i = 1, \ldots, n-1)$, where

$$
\begin{aligned}
f_0{}' &= S1_0 S3\left(\frac{I_{\max} K_{\mathrm{m}}}{(K_{\mathrm{m}} + C_{0,j+1} - C_{\min})^2} - v_0\right) + D1 + Q1\ I'_{h\,(0,j+1)}, \\
I'_{h\,(.,j+1)} &= \frac{\partial I_h(C_\ell)}{\partial C_\ell} = I_{\max_h} A_h \left(\frac{K_{\mathrm{m}_h} \frac{\partial C_{rh}}{\partial C_\ell}}{\left(C_{rh}(C_\ell) - C_{\min} + K_{\mathrm{m}_h}\right)^2}\right), \\
\frac{\partial C_{rh}}{\partial C_\ell} &= \frac{K_{\mathrm{m}_h}}{2}\left(1 + \frac{C_\ell - C_{\min} - Y + K_{\mathrm{m}_h}}{\sqrt{C^2_{\min} - 2C_{\min}(K_{\mathrm{m}_h} - Y + C_\ell) + K^2_{\mathrm{m}_h} + 2K_{\mathrm{m}_h}(Y + C_\ell) + (Y - C_\ell)^2}}\right).
\end{aligned}
$$

References

[1] S. Barber, J. Cushman, Nitrogen uptake model for agronomic crops, Modeling wastewater renovation: Land treatment. Wiley Interscience, New York (1981) 382–489.

[2] N. Macariola-See, H. J. Woodard, T. Schumacher, Field verification of the barber-cushman mechanistic phosphorus uptake model for maize, Journal of Plant Nutrition 26 (2003) 139–158. doi:10.1081/PLN-120016501.

[3] T. Adhikari, R. Rattan, Modelling zinc uptake by rice crop using a barber-cushman approach, Plant and Soil 227 (2000) 235–242.

[4] J. M. Kelly, S. A. Barber, G. S. Edwards, Modeling magnesium, phosphorus and potassium uptake by loblolly pine seedlings using a barber-cushman approach, Plant and Soil 139 (1992) 209–218. doi:10.1007/BF00009312.

[5] J. M. Kelly, J. Scarbrough, P. Mays, Hardwood seedling root and nutrient parameters for a model of nutrient uptake, Journal of Environmental Quality 30 (2001) 427–439. doi:10.2134/jeq2001.302427x.

[6] T. H. Mai, A. Schnepf, H. Vereecken, J. Vanderborght, Continuum multiscale model of root water and nutrient uptake from soil with explicit consideration of the 3d root architecture and the rhizosphere gradients, Plant and Soil 439 (2019) 273–292. doi:10.1007/s11104-018-3890-4.

[7] J. Postma, C. Kuppe, M. Owen, N. Mellor, M. Griffiths, M. Bennett, L. J.P., M. Watt, Opensimroot: Widening the scope and application of root architectural models, New Phytologist 215 (2017) 1274–1286. doi:10.1111/nph.14641.

[8] J. A. Postma, J. P. Lynch, Root cortical aerenchyma enhances the growth of maize on soils with suboptimal availability of nitrogen, phosphorus, and potassium, Plant Physiology 156 (2011) 1190–1201. doi:10.1104/pp.111.175489.

[9] J. A. Postma, J. P. Lynch, Complementarity in root architecture for nutrient uptake in ancient maize/bean and maize/bean/squash polycultures, Annals of Botany 110 (2012) 521–534. doi:10.1093/aob/mcs082.

[10] J. A. Postma, A. Dathe, J. P. Lynch, The optimal lateral root branching density for maize depends on nitrogen and phosphorus availability, Plant Physiology 166 (2014) 590–602. doi:10.1104/pp.113.233916.

[11] S. Itoh, S. A. Barber, A numerical solution of whole plant nutrient uptake for soil-root systems with root hairs, Plant and Soil 70 (1983) 403–413.

[12] J. H. Cushman, An analytical solution to solute transport near root surfaces for low initial concentration: I. Equations development1, Soil Science Society of America Journal 43 (1979) 1087. doi:10.2136/sssaj1979.03615995004300060005x.

[13] J. H. Cushman, The effect of a constant efflux on solute movement to a root, Plant and Soil 53 (1979) 303–317. doi:10.1007/BF02277865.

[14] J. Cushman, Analytical study of the effect of ion depletion (replenishment) caused by microbial activity near a root., Soil Science 129 (1980) 69–87. doi:10.1097/00010694-198002000-00001.

[15] J. H. Cushman, Completion of the list of analytical solutions for nutrient transport to roots: 1. exact linear models, Water Resources Research 16 (1980) 891–896. doi:10.1029/WR016i005p00891.

[16] M. T. Van Genuchten, Analytical solutions for chemical transport with simultaneous adsorption, zero-order production and first-order decay, Journal of Hydrology 49 (1981) 213–233. doi:10.1016/0022-1694(81)90214-6.

[17] T. Roose, A. Fowler, P. Darrah, A mathematical model of plant nutrient uptake, Journal of Mathematical Biology 42 (2001) 347–360. doi:10.1007/s002850000075.

[18] T. Roose, G. J. D. Kirk, The solution of convection–diffusion equations for solute transport to plant roots, Plant and Soil 316 (2009) 257–264. doi:10.1007/s11104-008-9777-z.

[19] Z. Ou, Approximate nutrient flux and concentration solutions of the nye-tinker-barber model by the perturbation expansion method, Journal of Theoretical Biology 476 (2019) 19–29. doi:10.1016/j.jtbi.2019.05.012.

[20] D. R. Bouldin, Mathematical description of diffusion processes in the soil-plant system 1, Soil Science Society of America Journal 25 (1961) 476–480. doi:10.2136/sssaj1961.03615995002500060018x.

[21] M. Huysmans, A. Dassargues, Review of the use of Péclet numbers to determine the relative importance of advection and diffusion in low permeability environments, Hydrogeology Journal 13 (2005) 895–904. doi:10.1007/s10040-004-0387-4.

[22] R. Courant, K. Friedrichs, H. Lewy, Über die partiellen differenzengleichungen der mathematischen physik, Mathematische Annalen 100 (1928) 32–74. doi:10.1007/BF01448839.

[23] J. Kunes, Dimensionless Physical Quantities in Science and Engineering, Elsevier, 2012.

[24] J. Passioura, M. Frere, Numerical analysis of the convection and diffusion of solutes to roots, Soil Research 5 (1967) 149–159. doi:10.1071/SR9670149.

[25] P. H. Nye, F. H. C. Marriott, A theoretical study of the distribution of substances around roots resulting from simultaneous diffusion and mass flow, Plant and Soil 30 (1969) 459–472. doi:10.1007/BF01881971.

[26] E. I. Newman, A. Watson, Microbial abundance in the rhizosphere: A computer model, Plant and Soil 48 (1977) 17–56. doi:10.1007/BF00015157.

[27] P. H. Nye, Changes of ph across the rhizosphere induced by roots, Plant and Soil 61 (1981) 7–26. doi:10.1007/BF02277359.

[28] J. Crank, P. Nicolson, A practical method for numerical evaluation of solutions of partial differential equations of the heat-conduction type, Mathematical Proceedings of the Cambridge Philosophical Society 43 (1947) 50–67. doi:10.1017/S0305004100023197.

[29] A. Boghi, T. Roose, G. J. D. Kirk, A model of uranium uptake by plant roots allowing for root-induced changes in the soil, Environmental Science & Technology 52 (2018) 3536–3545. doi:10.1021/acs.est.7b06136, pMID: 29466669.

[30] P. W. Leadley, J. F. Reynolds, F. S. Chapin, A model of nitrogen uptake by eriophorum vaginatum roots in the field: Ecological implications, Ecological Monographs 67 (1997) 1–22. doi:10.1890/0012-9615(1997)067[0001:AMONUB]2.0.CO;2.

[31] G. A. Roshania, G. Narayanasamyb, S. C. Dattab, Modelling potassium uptake by wheat, International Journal of Plant Production 3 (2009) 55–68.

[32] J. P. Baldwin, P. H. Nye, P. B. Tinker, Uptake of solutes by multiple root systems from soil, Plant and Soil 38 (1973) 621–635. doi:10.1007/BF00010701.

[33] C. W. Oosterlee, F. J. Gaspar, T. Washio, R. Wienands, Multigrid line smoothers for higher order upwind discretizations of convection-dominated problems, Journal of Computational Physics 139 (1998) 274–307. doi:10.1006/jcph.1997.5854.

[34] B. Van Leer, Upwind-difference methods for aerodynamics problems governed by the euler equations, in: Lectures in Appl. Math., 22, 1985, pp. 327–336.

[35] U. Trottenberg, C. Oosterlee, A. Schüller, Multigrid, Academic Press, 2001.

[36] B. Koren, Numerical methods for advection-diffusion problems, ed, CB Vreugdenhil & B. Koren (Braunschweig: Vieweg) 117 (1993).

[37] S. Lecheler, Numerische Strömungsberechnung: Schneller Einstieg durch ausführliche praxisrelevante Beispiele, Springer-Verlag, 2009.

[38] E. Hairer, S. P. Nørsett, G. Wanner, Solving ordinary differential equations I: Nonstiff problems, Springer Science & Business Media, 1993.

[39] J. R. Cash, A. H. Karp, A variable order runge-kutta method for initial value problems with rapidly varying right-hand sides, ACM Trans. Math. Softw. 16 (1990) 201–222. doi:10.1145/79505.79507.

[40] E. A. Celaya, J. J. A. Aguirrezabala, P. Chatzipantelidis, Implementation of an adaptive bdf2 formula and comparison with the matlab ode15s, Procedia Computer Science 29 (2014) 1014–1026. doi:10.1016/j.procs.2014.05.091, 2014 International Conference on Computational Science.

[41] P. Deuflhard, M. Weiser, Adaptive numerical solution of PDEs, De Gruyter Textbook, De Gruyter, 2012.

[42] C. A. J. Fletcher, Linear convection-dominated problems, Springer Berlin Heidelberg, Berlin, Heidelberg, 1998, pp. 276–330. doi:10.1007/978-3-642-58229-5_9.

[43] S. A. Barber, Soil nutrient bioavailability: A mechanistic approach, second ed., John Wiley & Sons, 1995.

[44] G. Eigenberger, J. Butt, A modified crank—nicolson technique with non-equidistant space steps, Chemical Engineering Science 31 (1976) 681–691. doi:10.1016/0009-2509(76)87011-X.

[45] J. D. Lambert, Numerical methods for ordinary differential systems: the initial value problem., Wiley, Chichester, 1991.

[46] A. E. Nakhi, Adaptive construction modelling within whole building dynamic simulation, Ph.D. thesis, University of Strathclyde, Glasgow, UK, 1995.

[47] H.-G. Roos, H. Schwetlick, Randwertaufgaben, Vieweg+Teubner Verlag, Wiesbaden, 1999, pp. 159–210. doi:10.1007/978-3-322-80008-4_8.

[48] C. Grossmann, Finite Difference Methods, Springer Berlin Heidelberg, Berlin, Heidelberg, 2007, pp. 23–124. doi:10.1007/978-3-540-71584-9_2.

[49] W. T. Vetterling, S. A. Teukolsky, W. H. Press, B. P. Flannery, Numerical Recipes in C: The Art of Scientific Computing, Cambridge University Press, 1992.